J Biomol NMR (2007) 38:47–55
DOI 10.1007/s10858-006-9138-2

ARTICLE

Sensitivity-optimized experiment for the measurement of residual dipolar couplings between amide protons

Paul Schanda · Ewen Lescop · Mirjam Falge · Rémy Sounier · Jérôme Boisbouvier · Bernhard Brutscher

Received: 26 October 2006 / Accepted: 20 December 2006 / Published online: 8 March 2007

Abstract High signal to noise is a necessity for the quantification of NMR spectral parameters to be translated into accurate and precise restraints on protein structure and dynamics. An important source of long-range structural information is obtained from ^{1}H–^{1}H residual dipolar couplings (RDCs) measured for weakly aligned molecules. For sensitivity reasons, such measurements are generally performed on highly deuterated protein samples. Here we show that high sensitivity is also obtained for protonated protein samples if the pulse schemes are optimized in terms of longitudinal relaxation efficiency and J-mismatch compensated coherence transfer. The new sensitivity-optimized quantitative J-correlation experiment yields important signal gains reaching factors of 1.5 to 8 for individual correlation peaks when compared to previously proposed pulse schemes.

Keywords Protein · Structure · Residual dipolar couplings · Fast NMR · HMQC · J-mismatch compensation · Longitudinal relaxation enhancement

Paul Schanda and Ewen Lescop contributed equally to this work.

P. Schanda · E. Lescop · M. Falge · R. Sounier · J. Boisbouvier · B. Brutscher (✉)
Institut de Biologie Structurale – Jean-Pierre Ebel, UMR5075 CNRS-CEA-UJF, 41, rue Jules Horowitz, 38027 Grenoble Cedex 1, France
e-mail: bernhard.brutscher@ibs.fr

J. Boisbouvier
e-mail: jerome.boisbouvier@ibs.fr

Introduction

Residual dipolar couplings (RDCs), measured in weakly aligned molecules in solution, provide an important source of structural information (Tjandra and Bax 1997; Prestegard et al. 2004; Blackledge 2005) that complement or replace more classical NMR data such as nuclear Overhauser effects (nOes) and scalar coupling constants (J). Whereas nOe-based distance restraints are affected by indirect spin interactions (spin diffusion), and J-coupling-derived torsion angles rely on empirical Karplus curves, RDCs directly reflect the interaction strength between two nuclear spins that can be translated into structural restraints of high accuracy using a well-known analytical formula. RDCs therefore provide access to more precise definition of local and long-range molecular structure. It has also been shown that RDCs, measured in several alignment media, are particularly attractive for RDC-based *de novo* protein fold determination (Kontaxis et al. 2005; Hus et al. 2001; Beraud et al. 2002), and the characterization of molecular dynamics at an atomic level occurring at time scales of pico- to milliseconds (Meiler et al. 2001; Bouvignies et al. 2005; Lakomek et al. 2005).

Nowadays RDCs are routinely measured between covalently attached nuclei, e.g. N–H, C–H, N–C, and C–C, mainly in the protein backbone, as part of the standard data set recorded for NMR structure elucidation. The distance and orientational information provided by long-range RDCs between more distant nuclei is still less exploited. It has been shown recently for proteins and nucleic acids that ^{1}H–^{1}H RDCs can be accurately measured between protons separated by more than 7 Å, provided that the ^{1}H spin coupling

network in these molecules is simplified by means of either deuteration, band-selective homonuclear decoupling, or both (Boisbouvier et al. 2003; Meier et al. 2003; Wu and Bax 2002). Here, we will focus on the measurement of long-range RDCs between amide protons in small to medium sized proteins. The sensitivity of the experimental schemes proposed so far greatly benefits from perdeuteration followed by back-protonation of the labile (amide) hydrogen sites. Most NMR experiments, commonly used for the study of small to medium-sized proteins, do not require perdeuteration. In order to make amide ^{1}H–^{1}H RDC measurements more attractive for fully protonated (or only partially deuterated) samples we have developed a new pulse sequence that provides greatly improved sensitivity over existing methods. Signal enhancements, ranging from a factor of 1.5 to 8, are observed for individual correlation peaks, as illustrated for ^{15}N labeled ubiquitin under weak alignment conditions.

Sensitivity-enhanced double ^{15}N-edited ^{1}H–^{1}H correlation experiment

In contrast to experiments for the measurement of one- or two bond couplings, long-range ^{1}H–^{1}H RDCs are most conveniently measured by a quantitative J-correlation experiment (Bax et al. 1994), where part of the magnetization is transferred from proton H^A to proton H^B yielding a cross peak at the resonance frequency of H^B and a diagonal peak at the frequency of H^A in the final spectrum. The spin coupling constant is then easily retrieved from the ratio of the measured intensities of cross- and diagonal peaks (see below). The new pulse sequence of Fig. 1a is a modified version of the Semi-Selective HMQC2 (SS-HMQC2) experiment (Wu and Bax 2002) that consists of two successive HMQC blocks sandwiching a COSY-type ^{1}H mixing pulse. In the following we will refer to our new experiment as BEST-Jcomp-HMQC2 (BEST: Band-selective-Excitation Short-Transient, Jcomp: J-mismatch compensated). Before describing in more detail the new features of BEST-Jcomp-HMQC2, we will briefly summarize the relevant coherence transfer pathways common to the double-HMQC experiment. Amide ^{1}H chemical shift, scalar and dipolar coupling evolutions with aliphatic protons are refocused by the band-selective 180° ^{1}H pulses applied in the middle of each HMQC building block. In contrast, H^N–H^N RDCs evolve during the transfer delay Δ_1 as $H^A{}_y \rightarrow H^A{}_y\cos(\pi D_{HH}\Delta_1) + 2H^A{}_xH^B{}_z \sin(\pi D_{HH}\Delta_1)$, where D_{HH} is the residual dipolar coupling constant between spins H^A and H^B and interactions with other amide protons are neglected. The following 90° ^{1}H pulse then converts $2H^A{}_xH^B{}_z$ to $-2H^A{}_zH^B{}_x$ while leaving $H^A{}_y$ (which gives rise to the diagonal peak) unaffected. During the subsequent Δ_2 transfer period, the antiphase coherence $-2H^A{}_zH^B{}_x$ partially refocuses to $H^B{}_y \sin(\pi D_{HH}\Delta_2)$ that is then detected as a cross peak. Remaining $2H^A{}_zH^B{}_x$ and $2H^A{}_xH^B{}_z$ coherences that are apparent as dispersive antiphase signals in the ^{1}H (ω_3) dimension of the spectrum can be suppressed by an additional z-filter element that will be explained in more detail below. Contrary to the experiment of Wu and Bax (2002), where ^{1}H antiphase suppression is an integral part of the pulse scheme, removing the z-filter element from the sequence of Fig. 1a does not alter the main coherence transfer pathways (see below). Therefore the experiment may also be performed without z-filter. During both ^{1}H–^{1}H dephasing times Δ_1 and Δ_2, the ^{15}N chemical shift of the covalently attached amide is labeled using HMQC-type ^{1}H–^{15}N correlation schemes. The residual dipolar coupling $D = D_{HH}$ is then obtained from the 4 peak intensities measured at positions (ω_1, ω_2, ω_3): $I^A_{cross}(\omega_N^A, \omega_N^B, \omega_H^B)$, $I^A_{diag}(\omega_N^A, \omega_N^A, \omega_H^A)$, $I^B_{cross}(\omega_N^B, \omega_N^A, \omega_H^A)$, $I^B_{diag}(\omega_N^B, \omega_N^B, \omega_H^B)$ using the following relation:

$$\frac{I^A_{cross}I^B_{cross}}{I^A_{diag}I^B_{diag}} = \frac{\lambda^2\sin^2(\pi D\Delta_1)\sin^2(\pi D\Delta_2)}{\{\lambda^2\cos^2(\pi D\Delta_1)\cos^2(\pi D\Delta_2)+2\lambda(1-\lambda)\cos(\pi D\Delta_1)\cos(\pi D\Delta_2)+(1-\lambda)^2\}} \quad (1)$$

with λ a correction factor taking into account the protonation level at the amide sites in the protein (Wu and Bax 2002), e.g. $\lambda = 0.9$ for a 10%/90% D_2O/H_2O mixture.

Solving Eq. [1] for a measured intensity ratio yields the magnitude of the D_{HH} coupling constant, given by

$$|D_{HH}| = \frac{\gamma_H^2\mu_0 h}{16\pi^3 r_{HH}^3}\left|A_a\left(3\cos^2\theta - 1\right) + \frac{3}{2}A_r\sin^2\theta\cos 2\varphi\right| \quad (2)$$

with A_a and A_r the axial and rhombic components of the alignment tensor, θ and ϕ the polar angles defining the H^N–H^N vector orientation with respect to the alignment frame, and r_{HH} the inter-proton distance.

The sensitivity of BEST-Jcomp-HMQC2 greatly benefits from two new features, longitudinal relaxation enhancement and J-mismatch compensation, that will be discussed in detail in the following.

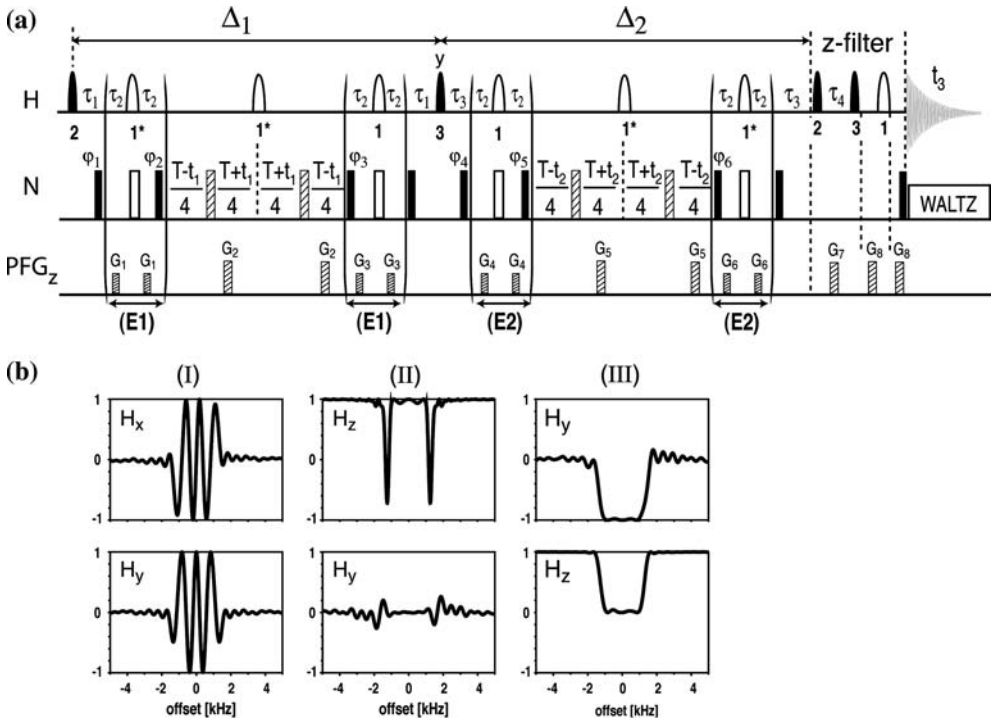

Fig. 1 (**a**) Pulse sequence of the 3D BEST-Jcomp-HMQC2 experiment for the measurement of amide ^{1}H–^{1}H residual dipolar couplings. The inserts labeled (E1) and (E2) correspond to J-mismatch compensation elements as explained in the text. The optional z-filter at the end suppresses $2H_xH_z$-type coherence prior to detection. All radio-frequency (rf) pulses are applied along the *x*-axis unless indicated. 90° and 180° rf pulses are represented by filled and open pulse symbols, respectively. The dashed ^{15}N pulses are broadband inversion pulses applied with a BIP-360-30-5 shape (Smith et al. 2001). All shaped ^{1}H pulses are centered at 8.2 ppm covering a band width of 4.0 ppm corresponding to the amide ^{1}H spectral region. The following shapes are used: (1) REBURP, (2) time-reversed EBURP2 (EBURP*), and (3) EBURP2 (Geen and Freeman 1991). For pairs of successive 180° rotations (1*) ISNOB5 pulses (Kupce et al. 1995) instead of REBURP are applied because of their cleaner band-selective inversion profile. The transfer delays are adjusted to $\tau_1 = 1/(2J_{NH})–\delta_1/2$, $\tau_2 = 1/(4J_{HN})–\delta_2/2$, $\tau_3 = 1/(2J_{NH})$, $\tau_4 = 1/(2J_{NH})–\delta_1$, and T≅30–60 ms, with δ_1 and δ_2 the lengths of the EBURP2 and REBURP pulses, respectively. The transfer delays Δ_1 and Δ_2 take into account ^{1}H–^{1}H coupling evolution during the selective pulses: $\Delta_1 = 2\tau_1 + 4\tau_2 + T$ and $\Delta_2 = 2\tau_3 + 4\tau_2 + T$. Pulsed field gradients, G_1–G_8 are applied along the *z*-axis (PFG_z) with a duration of 200 μs and field strengths ranging from 5–40 G/cm. Phase cycling: φ_1 = x,-x,x,-x, φ_2 = y,-y,-y,y, φ_3 = 2y,2(-y), φ_4 = x, φ_5 = 4y,4(-y), φ_6 = 4y,4(-y), and the receiver φ_{rec} = x,-x. Quadrature detection in the t_1 (t_2) dimension is obtained by simultaneous time-proportional phase incrementation of $\varphi_1(\varphi_4)$ and decrementation of $\varphi_2(\varphi_5)$ according to TPPI-STATES. The pulse sequence code (Varian) is available from the authors upon request. (**b**) Bloch simulations illustrating the effect of EBURP2 and time-reversed EBURP2 pulses in the pulse sequence (**a**). Coupling evolution has not been taken into account for the simulations. The plotted offset profiles represent the ^{1}H spin state after different pulse combinations starting from pure z-magnetization (H_z): (I) EBURP*$_x$, (II) EBURP*$_x$–Δ–180°–Δ-EBURP$_x$, and (III) EBURP*$_x$–Δ–180°–Δ–EBURP$_y$

Longitudinal relaxation enhancement

In slowly tumbling diamagnetic molecules such as proteins the efficiency of ^{1}H spin lattice relaxation is mainly determined by the dipolar-coupled ^{1}H spin network (^{1}H–^{1}H nOes). Therefore, if only a subset of protons is observed in a particular NMR experiment, spin-lattice relaxation can be enhanced by manipulating the remaining proton spins during the pulse sequence in a way that their spin state before detection is close to thermal equilibrium. The effective longitudinal spin-lattice relaxation of labile solvent-accessible amide ^{1}H is also influenced by chemical exchange with water hydrogens. Partial saturation of the water proton spins translates via this exchange mechanism to a reduced steady state polarization of the fast exchanging amides at the beginning of each scan. Again, longitudinal relaxation is enhanced when the water is in a relaxed state between subsequent scans. Shorter longitudinal relaxation times allow for higher repetition rates of the pulse sequence, and thus provide increased signal to noise (S/N) in a given amount of experimental time (higher sensitivity). Longitudinal relaxation enhancement has recently been successfully exploited for proteins in the context of resonance assignment experiments (Pervushin et al. 2002; Atreya and

Szyperski 2004; Diercks et al. 2005; Schanda et al. 2006b), ultrafast two-dimensional data acquisition (Schanda and Brutscher 2005; Schanda et al. 2005; Schanda and Brutscher 2006), and fast characterization of structural compactness and heterogeneity of polypeptide chains (Schanda et al. 2006a).

In the pulse sequence of Fig. 1a, only shaped ^{1}H pulses are applied that selectively manipulate amide ^{1}H while leaving aliphatic ^{1}H mostly unaffected. The BEST concept, consisting of the use of amide ^{1}H-selective pulses only, has been shown to yield superior results in terms of leaving aliphatic ^{1}H polarization unperturbed compared to hard-pulse-based sequences using additional selective ''flip-back'' pulses (Schanda et al. 2006b). In the sequence of Fig. 1a, a single 180° ^{1}H pulse is applied with a REBURP shape, whereas for pairs of consecutive 180° ^{1}H pulses ISNOB5 pulse shapes are preferred because of their better off-resonance performance. A time-reversed EBURP2 pulse (EBURP2*), initially optimized for flip-back purposes, is used for ^{1}H excitation. As illustrated by the Bloch simulations in Fig. 1b, EBURP2* leaves chemical shift evolution (and spin–spin coupling) active during half of the pulse duration thereby creating a linear phase gradient. This phase gradient is refocused during the subsequent 90° pulse applied with an EBURP2 shape and a 90° phase shift with respect to the EBURP2* pulse. An inphase H_y coherence is created for the component that has not evolved under dipolar coupling. At the same time the EBURP2 creates inphase H_x coherence from H_z, and flips back orthogonal transverse coherence along the z-axis (see Fig. 1b), thereby converting the antiphase coherence $2H^A{}_xH^B{}_z$ to $-2H^A{}_zH^B{}_x$. The combination EBURP2*–Δ –180°–Δ–EBURP2 allows efficient use of the relatively long pulse durations (on the order of 2 ms), and avoids general rotation 90° pulses that are known to be more sensitive to B_1-field inhomogeneities and pulse imperfections.

Figure 2 illustrates the effect of the BEST modifications on the sensitivity of the experiment for two protein samples at ^{1}H frequencies of 600 and 800 MHz: (a, c) 76-residue fully protonated ubiquitin and (b, d) a 167-residue fragment of the *Escherichia coli* sulfate reductase (SiR-FP18) deuterated at a level of ~75% (Sibille et al. 2005). 2D BEST-HMQC2 spectra were recorded without the J-mismatch compensation filters setting the effective evolution delays Δ_1 and Δ_2 to 26 ms. The average sensitivity (intensity per unit time) of BEST-HMQC2 is plotted as a function of the scan time (sum of pulse sequence duration and recovery delay), and compared to results obtained using the SS-HMQC2 sequence (Wu and Bax 2002) recorded under comparable conditions. As a result of the selective ^{1}H manipulation in BEST-HMQC2 the maximum in the sensitivity curves shifts towards shorter scan times, reflecting the significant decrease in effective longitudinal relaxation times. For protonated ubiquitin, scan times of ~600 ms are optimal, whereas for the highly deuterated sample of SiR-FP18 a scan time of ~1.5 s provides highest S/N ratios. These optimal repetition rates depend only little on the magnetic field strength. An average sensitivity gain of a factor of ~2, and individual gains of up to a factor of 4 (data not

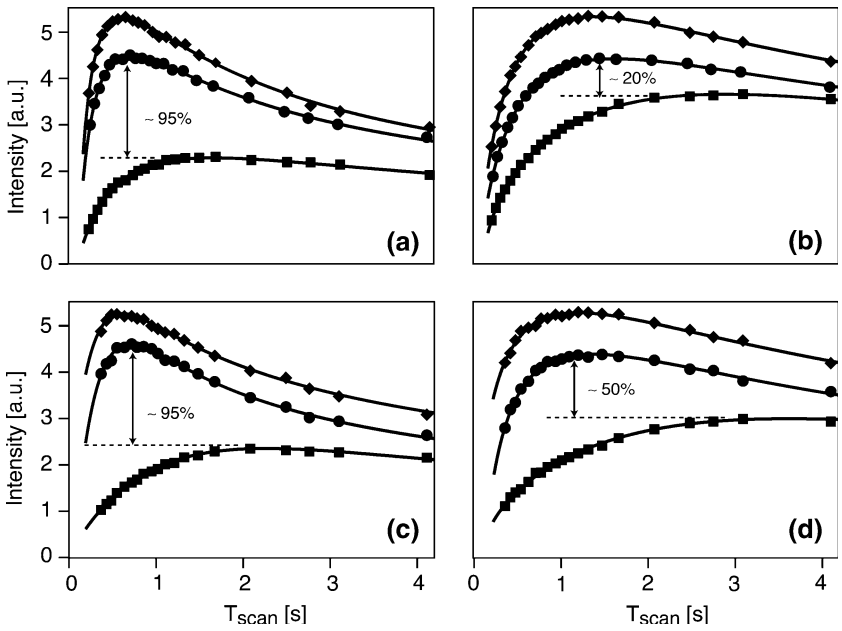

Fig. 2 Average S/N ratios per unit time (intensity) plotted as a function of the scan time (pulse sequence duration plus recycle delay) obtained with the BEST-Jcomp HMQC sequence without z-filter (diamonds), with additional z-filter (circles), and using the SS-HMQC2 sequence of Wu and Bax (squares) for fully protonated ubiquitin at (**a**) 600 MHz and (**c**) 800 MHz ^{1}H frequency, and for ~75% partially deuterated SiR-FP18 at (**b**) 600 MHz and (**d**) 800 MHz ^{1}H frequency. Intensities were obtained by adding the peak intensities of all detected amide (excluding NH_2) correlation peaks observed in the 2D spectra

shown) are observed for ubiquitin if the scan times of both experiments are optimized independently. Even for the deuterated sample of SiR-FP18, an average sensitivity gain of 20% at 600 MHz and 50% at 800 MHz is obtained. This observation can be explained by the fact that most methyl groups remain protonated at least at one of the three methyl hydrogen sites. ^{1}H–^{1}H spin diffusion to methyl groups then still allows quite efficient energy dissipation at these sites of high mobility (methyl rotation). Additionally, and in contrast to the SS-HMQC2 experiment, water polarization is left unperturbed rather than dephased, which also contributes to faster effective relaxation of the exchangeable amide protons. Even higher sensitivity gains are observed in the fast pulsing regime when using short recycle delays for both SS-HMQC2 and BEST-HMQC2 experiments. This may be relevant for situations where short overall acquisition times become important, e.g. for sample stability reasons.

J-mismatch compensation

Each of the two HMQC building blocks in the sequence of Fig. 1a requires the adjustment of two transfer delays $\tau = 1/(2J_{NH})$, where J_{NH} is the heteronuclear coupling constant between amide ^{1}H and ^{15}N. While the scalar J couplings are quite uniform along the polypeptide chain with very little variation from one amide site to another, in weakly aligned molecules the RDC adds to the J coupling resulting in effective spin coupling constants $J_{NH}^{eff} = J_{NH} + D_{NH}$ that cover a range of typically ±20–40% with respect to the mean value. It is therefore no longer possible to adjust the τ delays for all amide sites simultaneously, resulting in a sensitivity loss that depends on the degree of J-mismatch $f_{NH}^{Jmis} = 2\tau J_{NH}^{eff}$.

In a standard HMQC experiment the main coherence transfer pathway (P_I) is as follows:

$$H_y \xrightarrow{J_{NH}^{eff}} 2H_xN_y\ (t_1) \xrightarrow{J_{NH}^{eff}} H_y\ \sin^2\left(\pi f_{NH}^{Jmis}/2\right) \tag{3}$$

The efficiency of the heteronuclear transfer steps, given by $\sin^2\left(\pi f_{NH}^{Jmis}/2\right)$ neglecting spin relaxation, translates into a signal loss of ~20% for a J-mismatch of $f_{NH}^{Jmis} = 0.7$ or 1.3 (see Fig. 3). In order to increase the performance of the HMQC sequence for partially aligned protein samples, J-mismatch compensation elements (denoted (E1) and (E2) in the sequence of Fig. 1a) are inserted. The J-mismatch compensation technique used here is conceptually similar to previously proposed ''broadband INEPT'' schemes (Nielsen et al. 1989; Wimperis and Bodenhausen 1986). J-mismatch compensation allows recovering part of the ''lost'' magnetization by creating a second coherence transfer pathway (P_{II}) that adds to the detected NMR signal:

$$\begin{aligned} H_y &\xrightarrow{J_{NH}^{eff}} 2H_xN_x\ (t_1) \\ &\xrightarrow{J_{NH}^{eff}} H_y\ \cos^2\left(\pi f_{NH}^{Jmis}/2\right)\sin^2\left(\pi f_{NH}^{Jmis}/2\right) \end{aligned} \tag{4}$$

The transfer efficiency in J-mismatch compensated HMQC is then given by the sum of the two pathways P_I and P_{II}. In the J-mismatch range $0.7 < f_{NH}^{Jmis} < 1.3$ the ^{1}H–^{15}N transfer becomes almost independent of the effective coupling constant J_{NH}^{eff} with transfer efficiencies of more than 0.95 over the whole range (Fig. 3). The amide ^{1}H–^{1}H coupling evolution is not affected by these additional pulse sequence elements because no 90° ^{1}H pulse is required. The J-mismatch compensation elements can thus be inserted in the ^{1}H–^{1}H coupling evolution periods of the BEST-HMQC blocks. Therefore, no additional delays are required and the improved heteronuclear transfer efficiency of the HMQC blocks directly translates into intensity gains for the cross- and diagonal peaks depending on the

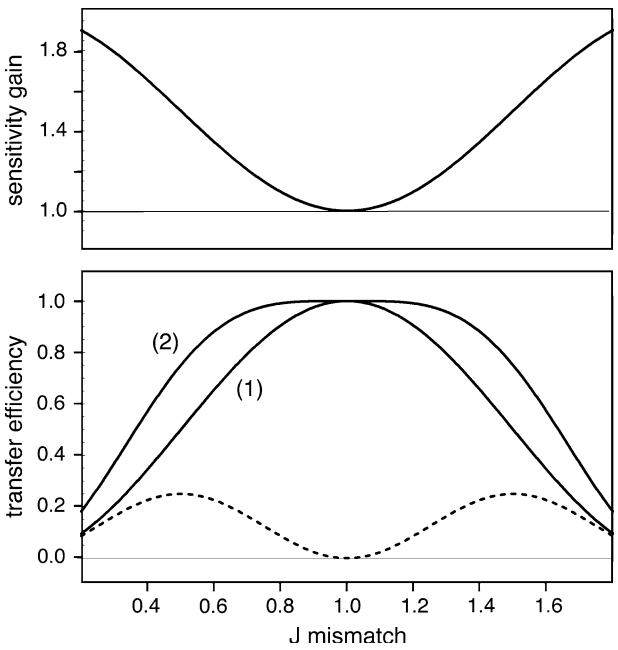

Fig. 3 Simulations of ^{1}H–^{15}N transfer efficiencies (see Eqs. [3] and [4]) in HMQC-type experiments with (2) and without (1) the additional J-mismatch compensation elements of Fig. 1a. The transfer efficiency of the additional coherence transfer pathway (P_{II}) created by the J-mismatch compensation elements is plotted as a dashed line. In addition, the expected signal gain for a single HMQC block as a function of J-mismatch is shown on top

J-mismatch of the involved amide groups. The only price to pay for the J-mismatch compensation, besides a few additional pulses, is a reduction (by ~11 ms) in the available maximal t_1 and t_2 evolution times. This however does not present a strong limitation as long as transfer delays $\Delta_1, \Delta_2 > 30$ ms are chosen for the amide ^{1}H–^{1}H coupling evolution.

Artefact suppression using an additional z-filter

To suppress undesired antiphase $2H_zH_x$ coherences before detection, while leaving inphase H_y coherence unperturbed, an optional z-filter element can be used. In short, the filter works as follows: the inphase H_y coherence is stored along the *z*-axis by a 90° EBURP2* pulse while antiphase $2H_xH_z$ coherence is converted to zero-quantum (ZQ) and double-quantum (DQ) coherences by the same pulse. The DQ coherence is destroyed by a pulsed field gradient. The ZQ coherence, that remains unaffected by the gradient pulse, evolves during a delay $1/2J_{NH}$ into $8H_+H\_N_zN_z$-type coherence that is not detected in the presence of ^{15}N decoupling during data acquisition. The use of a high-performance ^{15}N composite decoupling sequence, such as WALTZ-16, is important to avoid partial detection of undesired coherence transfer pathways resulting in phase distortions in the ^{1}H dimension. The subsequent EBURP2 pulse then converts H_z to H_y for final detection. Finally, a WATERGATE sequence (Piotto et al. 1992) is added for water suppression purposes.

Experimental results

The performance of the BEST-Jcomp-HMQC2 experiment has been tested on a 1.25 mM sample of fully protonated ^{15}N-labeled ubiquitin. To create a weak alignment in the magnetic field, the ubiquitin sample was dissolved in a 15% w/v DMPC/DHPC mixture at a molar ratio of 3:1. The pH of the sample was adjusted to 6.6 in a 10 mM phosphate buffer. The resulting molecular alignment tensor, characterized on the basis of a set of D_{NH} coupling constants measured from IPAP-HSQC spectra (Andersson et al. 1998; Ottiger et al. 1998) and the ubiquitin solution structure (pdb entry 1D3Z), showed an axial component of $A_a = 17.8\ 10^{-4}$ and a rhombic component of $A_r = 2.6\ 10^{-4}$. Under these alignment conditions the J-mismatch for individual amide sites ranged from 0.6 to 1.3 assuming a scalar coupling constant $J_{NH} = 92$ Hz. All spectra were acquired at 800 MHz ^{1}H frequency and 28°C sample temperature on a Varian INOVA spectrometer equipped with a cryogenic triple-resonance probe and shielded z-gradients. 3D spectra were recorded using different options of the pulse sequence displayed in Fig. 1a: with/without J-mismatch compensation, and with/without z-filter. In addition, a SS-HMQC2 spectrum (Wu and Bax 2002) was acquired for comparison using identical acquisition parameters except for the interscan delay, which was set to 450 ms in BEST-HMQC2 and to 1.4 s in SS-HMQC2 for optimal sensitivity in both experiments. Examples of 2D (ω_1, ω_2) strips extracted from these data sets are shown in Fig. 4a. On average, a sensitivity gain of approximately a factor of 2 is obtained from longitudinal relaxation enhancement when using BEST-Jcomp-HMQC2 instead of SS-HMQC2. This gain, however, is not uniform along the peptide chain and enhancement factors of 3 to 5 are observed for amide groups in the hydrophobic core of the protein characterized by a high local proton density and little internal dynamics. Interestingly, these are also the molecular regions where the most useful long-range structural information is obtained, as illustrated for the β-sheet structure of ubiquitin (Fig. 4b). J-mismatch compensation yields significant further signal enhancements for amide groups with large D_{NH} couplings. Sensitivity gains of up to a factor of 2 are observed when adding the J-mismatch compensation elements for cross and diagonal peaks were both amide groups involved in the correlation show large J-mismatch. The combination of both effects yields enhancement factors of the S/N ratio for individual correlation peaks in the range of ~1.5 to 8. The increased sensitivity allowed us to quantify additional peaks and thus obtain more structural restraints as compared to the SS-HMQC2 experiment. In addition to the 113 cross peaks that are observed in both experiments 41 additional cross peaks with intensities above a cutoff level of 3 times the noise level could be quantified. Exceptions are correlations between amide ^{1}H and the NH_2 groups of Asn and Gln side chains. These cross peaks have significantly reduced intensity in BEST-Jcomp-HMQC2 because of the additional J_{NH} coupling evolution of $2N_yH_x$-type coherence during the J-compensation pulse sequence elements (see residue L15 in Fig. 4a). Figure 5a shows the correlation of D_{HH} values extracted from 3D spectra measured using the SS-HMQC2 and BEST-Jcomp-HMQC2 sequences, illustrating that the same level of accuracy is obtained from the two experiments, although with a significantly higher precision for the sensitivity-optimized BEST-Jcomp-HMQC2 version.

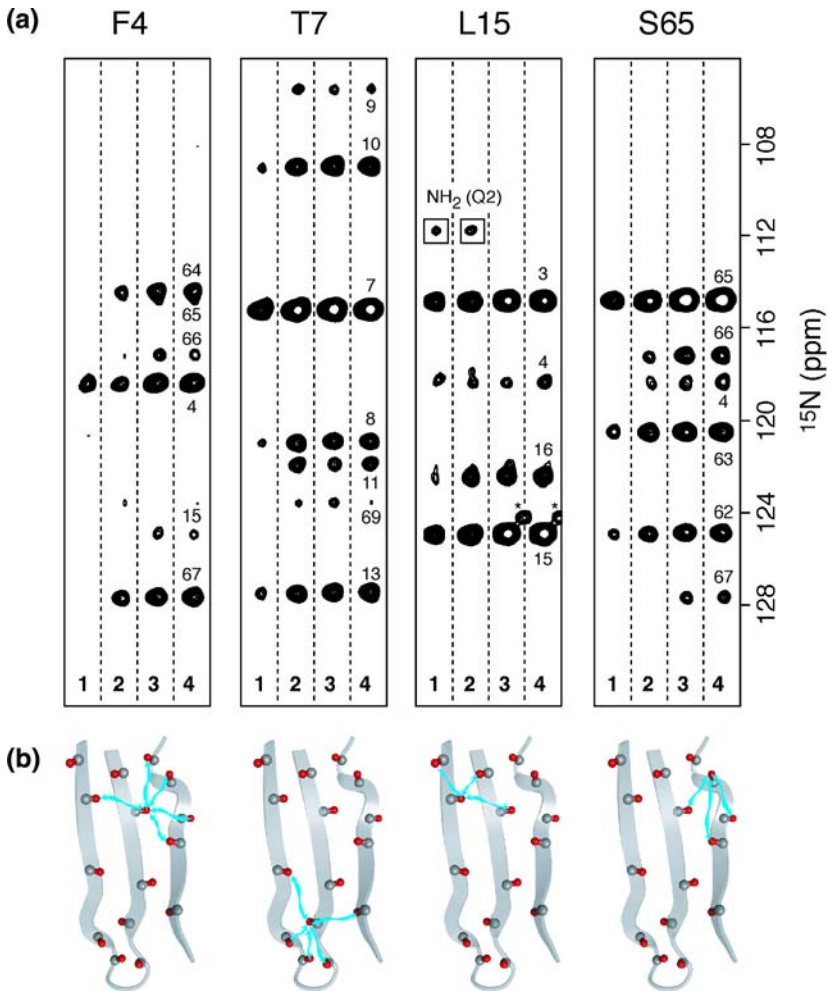

Fig. 4 2D ^{15}N (ω_1)–^{15}N (ω_2) strips extracted at the amide ^{1}H (ω_3) frequency of several residues in the β-sheet of ubiquitin. 3D data sets were recorded at 800 MHz (28°C) on a sample of ^{15}N-labelled, fully protonated ubiquitin dissolved in a DMPC/DHPC mixture. The results obtained with the following pulse sequences are shown: (1) SS-HMQC2, (2) BEST-HMQC2 without J-mismatch compensation and z-filter, (3) BEST-Jcomp-HMQC2 with additional J-mismatch compensation, and (4) BEST-Jcomp-HMQC2 with J-mismatch compensation and z-filter. For all experiments the ^{1}H–^{1}H transfer delays (corresponding to Δ_1 and Δ_2 in the sequence of Fig. 1a) were adjusted to 41 ms. 43 (t_1) × 43 (t_2) × 400(t_3) complex points were recorded for spectral widths of 2400 Hz (ω_1), 2400 Hz (ω_2) and 10000 Hz (ω_3). Optimal recycle delays were used for all experiments: 450 ms for BEST-Jcomp-HMQC2, and 1.4 s for SS-HMQC2. The total acquisition time was 10 h for the BEST experiments, and 24 h for the SS-HMQC2 spectrum. The intensities in the SS-HMQC2 spectrum were scaled by a factor 0.65 to account for the unequal experimental times. A star indicates a residual peak from another ^{1}H plane (residue). (**b**) Schematic drawing of the β-sheet structure in ubiquitin. The arrows indicate amide pairs for which RDCs could be measured from the spectral regions displayed in (**a**), illustrating that important long-range structural information is obtained from these data

We have also experimentally evaluated the effect of the additional z-filter element on the overall sensitivity of the BEST-Jcomp-HMQC2 experiment and the accuracy of the measured amide ^{1}H–^{1}H RDCs. Overall the intensity of most correlation peaks recorded with the additional z-filter is slightly reduced, by about 10–15% in the case of the weakly aligned ubiquitin sample used for this study (Fig. 4a), which is in agreement with the data shown in Fig. 2. There are two possible sources of signal losses: first, and probably most importantly, ^{1}H longitudinal relaxation during the z-filter element and ^{1}H transverse relaxation during the WATERGATE sequence of ~2 ms duration; second, as can be seen from Fig. 2, the optimal scan time is slightly shifted towards longer delays as compared to the experiment without the z-filter element, indicating that the additional pulses decrease the steady-state polarization of the aliphatic protons, and thus the sensitivity of the experiment. The small intensity increase observed for some cross peaks is explained by

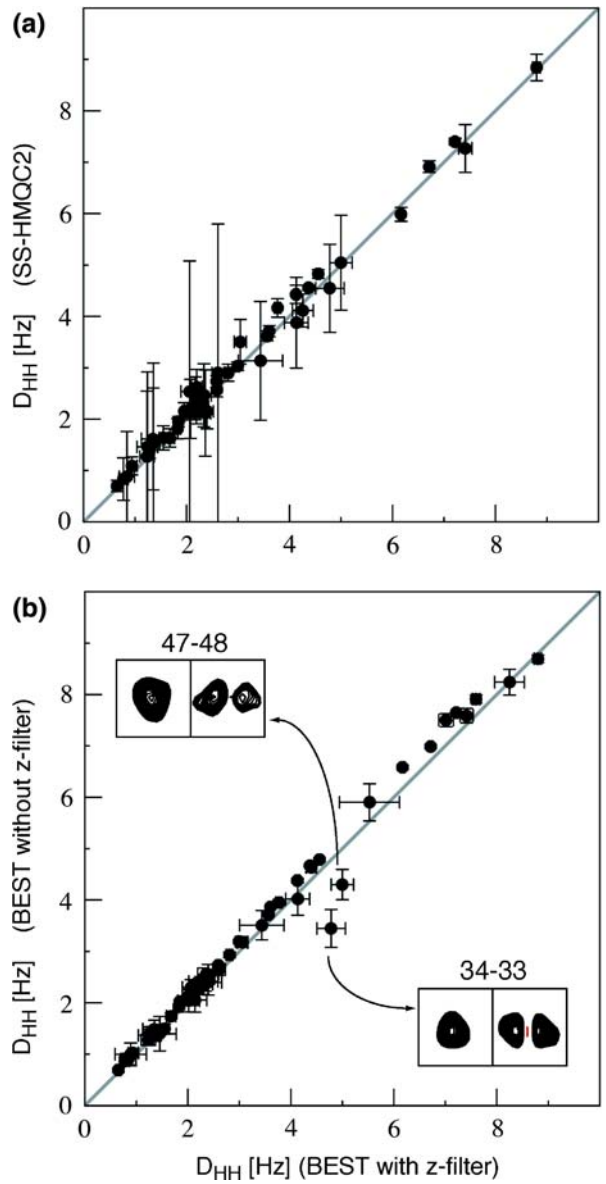

Fig. 5 (**a**) Correlation plot of amide ^{1}H–^{1}H RDCs measured using the BEST-Jcomp-HMQC2 sequence of Fig. 1a (*x*-axis) and SS-HMQC2 (Wu and Bax 2002) (*y*-axis). The total acquisition time was 10 h for BEST-Jcomp-HMQC2 and 24 h for SS-HMQC2. (**b**) Correlation plot of amide ^{1}H–^{1}H RDCs extracted from 3D BEST-Jcomp-HMQC2 spectra recorded with (*x*-axis) and without (*y*-axis) the additional z-filter. The experimental error bars were estimated on the basis of intensity uncertainties of 1.5 times the noise level. (**b**) The absolute values of the D_{HH} coupling constants were extracted from a single spectrum. Therefore all D_{HH} couplings were assumed to be in the 0 to 1/2Δ = 12.2 Hz range ($\Delta = \Delta_1 = \Delta_2$). The periodicity of the trigonometric functions in Eq. [1] does not allow the distinction between coupling constants *D* and 1/Δ -D. In order to solve this ambiguity a second data set recorded using a different transfer delay Δ is required. The inserts in (**b**) show ^{1}H line shape distortions observed for some cross peaks (right spectrum) that are completely removed by addition of the z-filter (left spectrum)

the removal of artifacts with negative intensity in the $\omega_3(^1\text{H})$ dimension. The difference in the RDC values extracted from the two experiments recorded with and without z-filter is surprisingly small for most of the observed correlations (Fig. 5b), indicating that also without the z-filter meaningful structural restraints can be obtained. Only a few peaks show significant distortions along the ^{1}H dimension (see Inserts in Figs. 5b) that result in erroneous peak intensities and thus stronger deviations in the measured D_{HH} coupling constants. These peak distortions are absent in the spectra recorded with the additional z-filter illustrating that the antiphase $2H_xH_z$ coherence is efficiently suppressed. The z-filtered version of the experiment thus yields higher accuracy at the expense of a small loss in sensitivity. However, the outliers are easily identified from inspection of the peak shape and accurate coupling constants can also be obtained from the experiment without the z-filter element if these peaks are manually removed from the analysis.

Conclusions

We have presented BEST-Jcomp-HMQC2, a new pulse sequence that allows accurate measurement of amide ^{1}H–^{1}H residual dipolar couplings in weakly aligned proteins. ^{1}H–^{1}H RDC measurements provide important long-range restraints for NMR structure determination. This information is available immediately after backbone resonance assignment without the need for any additional tedious side chain resonance assignment or NOE analysis. ^{1}H–^{1}H RDCs are therefore especially useful in the context of fast *de novo* fold elucidation using only a limited set of NMR-derived structural restraints. It has been shown recently (Bouvignies et al. 2006) that high structural precision is obtained by combining local orientational information from RDCs between covalently-bound nuclei in the protein backbone with long-range translational and orientational information from amide ^{1}H–^{1}H RDCs. The high sensitivity provided by the BEST-Jcomp-HMQC2 experiment makes it attractive to measure amide ^{1}H–^{1}H RDCs on a routine basis for partially aligned protein samples without the need for (per)deuteration.

Acknowledgments This work was supported by the Commissariat à l'Energie Atomique, the Centre National de la Recherche Scientifique, the French Research Agency (ANR), Human Frontier Science Program Organization and the European Commission (EU-NMR). P.S. and R.S. acknowledge support from the French ministry of education, research, and technology.

We thank Beate Bersch, Isabel Ayala, and Jacques Covès (IBS Grenoble) for the preparation of the isotope-labeled protein samples.

References

Andersson P, Weigelt J, Otting G (1998) Spin-state selection filters for the measurement of heteronuclear one-bond coupling constants. J Biomol NMR 12:435–441

Atreya HS, Szyperski T (2004) G-matrix Fourier transform NMR spectroscopy for complete protein resonance assignment. Proc Natl Acad Sci USA 101:9642–9647

Bax A, Vuister GW, Grzesiek S, Delaglio F, Wang AC, Tschudin R, Zhu G (1994) Measurement of homo- and heteronuclear J couplings from quantitative J correlation. Methods Enzymol 239, Pt C:79–105

Beraud S, Bersch B, Brutscher B, Gans P, Barras F, Blackledge M (2002) Direct structure determination using residual dipolar couplings: reaction-site conformation of methionine sulfoxide reductase in solution. J Am Chem Soc 124:13709–13715

Blackledge M (2005) Recent progress in the study of biomolecular structure and dynamics in solution from residual dipolar couplings. Prog Nucl Magn Reson 46:23–61

Boisbouvier J, Delaglio F, Bax A (2003) Direct observation of dipolar couplings between distant protons in weekly aligned nucleic acids. Proc Natl Acad Sci USA 100:11333–11338

Bouvignies G, Bernado P, Meier S, Cho K, Grzesiek S, Brüschweiler R, Blackledge M (2005) Identification of slow correlated motions in proteins using residual dipolar and hydrogen-bond scalar couplings. Proc Natl Acad Sci USA 102:13885–13890

Bouvignies G, Meier S, Grzesiek S, Blackledge M (2006) Ultrahigh-resolution backbone structure of perdeuterated protein GB1 using residual dipolar couplings from two alignment media. Angew Chem Int Ed Engl 45:8166–8169

Diercks T, Daniels M, Kaptein R (2005) Extended flip-back schemes for sensitivity enhancement in multidimensional HSQC-type out-and-back experiments. J Biomol NMR 33:243–259

Geen H, Freeman R (1991) Band-selective radiofrequency pulses. J Magn Reson 93:93–141

Hus JC, Marion D, Blackledge M (2001) Determination of protein backbone structure using only residual dipolar couplings. J Am Chem Soc 123:1541–1542

Kontaxis G, Delaglio F, Bax A (2005) Molecular fragment replacement approach to protein structure determination by chemical shift and dipolar homology database mining. Methods Enzymol 394:42–78

Kupce E, Boyd J, Campbell ID (1995) Short selective pulses for biochemical applications. J Magn Reson B 106:300–303

Lakomek NA, Fares C, Becker S, Carlomagno T, Meiler J, Griesinger C (2005) Side-chain orientation and hydrogen-bonding imprint supra-tau(c) motion on the protein backbone of ubiquitin. Angew Chem Int Ed Engl 44:7776–7778

Meier S, Haussinger D, Jensen P, Rogowski M, Grzesiek S (2003) High-accuracy residual 1HN–13C and 1HN–1HN dipolar couplings in perdeuterated proteins. J Am Chem Soc 125:44–45

Meiler J, Prompers JJ, Peti W, Griesinger C, Brüschweiler R (2001) Model-free approach to the dynamic interpretation of residual dipolar couplings in globular proteins. J Am Chem Soc 123:6098–6107

Nielsen NC, Bildsoe H, Jakobsen HJ, Sorensen OW (1989) Composite refocusing sequences and their application for sensitivity enhancement and multiplicity filtration in INEPT and 2D correlation spectroscopy. J Magn Reson 85:359–380

Ottiger M, Delaglio F, Bax A (1998) Measurement of J and dipolar couplings from simplified two-dimensional NMR spectra. J Magn Reson 131:373–378

Pervushin K, Vogeli B, Eletsky A (2002) Longitudinal (1)H relaxation optimization in TROSY NMR spectroscopy. J Am Chem Soc 124:12898–12902

Piotto M, Saudek V, Sklenar V (1992) Gradient-tailored excitation for single-quantum NMR spectroscopy of aqueous solutions. J Biomol NMR 2:661–665

Prestegard JH, Bougault CM, Kishore AI (2004) Residual dipolar couplings in structure determination of biomolecules. Chem Rev 104:3519–3540

Schanda P, Brutscher B (2005) Very fast two-dimensional NMR spectroscopy for real-time investigation of dynamic events in proteins on the time scale of seconds. J Am Chem Soc 127:8014–8015

Schanda P, Brutscher B (2006) Hadamard frequency-encoded SOFAST-HMQC for ultrafast two-dimensional protein NMR. J Magn Reson 178:334–339

Schanda P, Kupce E, Brutscher B (2005) SOFAST-HMQC experiments for recording two-dimensional heteronculear correlation spectra of proteins within a few seconds. J Biomol NMR 33:199–211

Schanda P, Forge V, Brutscher B (2006a) HET-SOFAST NMR for fast detection of structural compactness and heterogeneity along polypeptide chains. Magn Reson Chem 44:S177–S184

Schanda P, van Melckebeke H, Brutscher B (2006b) Speeding up three-dimensional protein NMR experiments to a few minutes. J Am Chem Soc 128:9042–9043

Sibille N, Blackledge M, Brutscher B, Coves J, Bersch B (2005) Solution structure of the sulfite reductase flavodoxin-like domain from *Escherichia coli*. Biochemistry 44:9086–9095

Smith MA, Hu H, Shaka AJ (2001) Improved broadband inversion performance for NMR in liquids. J Magn Reson 151:269–283

Tjandra N, Bax A (1997) Direct measurement of distances and angles in biomolecules by NMR in a dilute liquid crystalline medium. Science 278:1111–1114

Wimperis S, Bodenhausen G (1986) Heteronuclear coherence transfer over a range of coupling constants. A broadband-INEPT experiment. J Magn Reson 69:264–282

Wu ZR, Bax A (2002) Measurement of long-range ^{1}H–^{1}H dipolar couplings in weakly aligned proteins. J Am Chem Soc 124:9672–9673